# Spectroscopic Properties of $Pr^{3+}$ Ions in a $PbWO_4$ Single Crystal

**Yanlin Huang,[†] Taiju Tsuboi,[‡] and Hyo Jin Seo*[,§]**

*School of Material Engineering, Soochow University, 178 GanJiang East Road, Suzhou, 215021, P. R. China, Faculty of Engineering, Kyoto Sangyo University, Kamigamo, Kita-Ku, Kyoto 603-8555, Japan, and Department of Physics, Pukyong National University, Busan 608-737, Republic of Korea*

*Received: December 22, 2007; Revised Manuscript Received: April 9, 2008*

Site-selective fluorescence laser spectroscopy of $Pr^{3+}$ ions in lead tungstate single crystal were investigated at temperatures from 10 to 300 K. The site-selective emission spectra and fluorescence decays from the $^3P_J$ ($J = 0, 1, 2$) and $^1D_2$ states were analyzed. The $^3P_J$ ($J = 0, 1, 2$) level shows its predominantly radioactive character with the typical greenish-blue luminescence ascribed to $^3P_J$ transition. The emission from the $^1D_2$ level is only observed when this level is directly excited. The decay kinetic of the $^1D_2$ level was measured under site-selective excitation and discussed in terms of cross-relaxation. The up-conversion emission from levels $^3P_1$ and $^3P_0$ following excitation of the $^1D_2$ state was observed in the $PbWO_4$ crystal between 10 and 300 K. The main up-conversion mechanism, together with the understanding the quenching of the $^1D_2$ fluorescence in this $Pr^{3+}$ heavily doped $PbWO_4$ were discussed. The presence of the complex structures of the emission spectra and different decay profiles indicate that several processes contribute to the quenching of the $^1D_2$ fluorescence of $Pr^{3+}$ ions. It was found that the up-conversion fluorescence intensity had a quadratic dependence on the laser input power. The temporal behavior of the up converted emission indicates that an energy-transfer up-conversion is the dominant process.

## I. Introduction

In the past ten years, an extensive R&D program has been carried out by the Compact Muon Solenoid (CMS) experiment in developing lead tungstate crystals, $PbWO_4$ (PWO), for Large Hadron Collider (LHC) in CERN.[1] $PbWO_4$ crystal has been chosen as scintillating crystal because of its high density, short radiation length, and fast decay time.[2] To effectively improve the scintillating properties of $PbWO_4$, extensive researches have been performed by doping or codoping with the impurity ions, especially the trivalent rare earth ($RE^{3+}$) ions.[3]

$PbWO_4$ with Scheelite crystal structure shows not only rich luminescence phenomena[4–6] but also many specialties, e.g., rather low cost crystal growth of large size, a high refractive index, and chemical stability. In recent years, many researchers paid attention to the luminescence properties of $RE^{3+}$-doped $PbWO_4$. Especially Kaminskii et al. have carried out the detailed investigations on the Raman spectra and Raman laser of $PbWO_4$.[7,8] They obtained the total Stokes conversion efficiency beyond 50 %. They also reported the pulsed and continuous wave laser actions in $Nd^{3+}$-doped $PbWO_4$ crystal. On the other hand, Chen et al. have realized the self-stimulating Raman laser of $Nd^{3+}$-doped $PbWO_4$ crystal with 56 % optical frequency conversion efficiency.[5]

Trivalent praseodymium ion $Pr^{3+}$ with $4f^2$ configuration is an attractive lasing activator, which gives rise to stimulated emission (SE) at a wide wavelength range from 0.48 to 7.24 $\mu$m (see an excellent review article by Kaminskii[10]). $Pr^{3+}$-doped crystals can show SE generations at orange, red, and deep red, and IR spectral ranges at room temperature by a Xe flashlamp. For example, SE generation at 1.34 $\mu$m due to $^1G_4 \rightarrow {}^3H_5$ is widely used as praseodymium fiberglass lasers and amplifiers.[11,12] On the other hand SE generation at about 3.6 $\mu$m due to $^1G_4 \rightarrow {}^3F_4$ is known as laser with the longest lasing wavelength of various Xe-flashlamp-pumped crystalline lasers.[10] Besides the $^1G_4$ state, the $^1D_2$ manifold of $Pr^{3+}$ ions presents also a laser state. In $Pr^{3+}$-doped aluminosilicate glass fiber, the $^1D_2$ level gives laser emission at around 1050 nm due to the transition from the $^1D_2$ state to the $^3F_3$ and $^3F_4$ states.[13] Kaminskii et al. reported the low-threshold 1 $\mu$m SE that was excited with Xe-flash lamp-pumping at the $^1D_2$ state at 300 K in $Pr^{3+}$-doped $YAlO_3$ crystals.[14] A new laser emission due to $^1D_2 \rightarrow {}^1G_4$ is observed at 1.5 $\mu$m.[15] This emission is expected to be useful for the optical communications because of coincidence with low-loss range of current silica optical communication fiber. Laser action at 1.5 $\mu$m becomes important because direct "red" LD pumping into the $^1D_2$ state is possible.[10] It is noted that the intermanifold luminescence branching ratios of two SE channels ($^1D_2 \rightarrow {}^1F_3$ and $^1D_2 \rightarrow {}^1G_4$) were found to be rather high .[16]

Various studies have been made for the luminescence of $Pr^{3+}$-doped $PbWO_4$ crystal, e.g., luminescence under ultraviolet (UV) or X-ray excitation, and efficient energy transfer from the host $PbWO_4$ to the $Pr^{3+}$ ions.[4,17,18] Quantum cutting was also reported in $Pr^{3+}$-doped $PbWO_4$, which consists of the $^1S_0 \rightarrow {}^1D_2$ and $^1D_2 \rightarrow {}^3H_4$ transitions. Energy transfer between the $Pr^{3+}$ ions and the host crystal can convert the UV emission from the $^1S_0 \rightarrow {}^1D_2$ transition into a visible emissions from the $^3P_J$ ($J = 0$, 1) and $^1D_2$ multiplets in the range 490−650 nm.[19]

Although many laser action and spectroscopy studies have been made on $Pr^{3+}$-doped $PbWO_4$, detailed study has not been done for luminescence decay processes of $Pr^{3+}$ ions in $PbWO_4$ crystal. This work mainly focuses on the time-resolved luminescence properties by site selective excitation not only at room temperature but also at low temperatures such as 10 K, including emission spectrum and lifetime measurements, and the lumi-

* Corresponding author. E-mail: hjseo@pknu.ac.kr. Fax: 82-51-611-6357.
[†] Soochow University.
[‡] Kyoto Sangyo University.
[§] Pukyong National University.

10.1021/jp712030q CCC: $40.75 
Published on Web 06/11/2008

nescence decay kinetics. Especially the luminescence spectra and decay times related to the $^1D_2$ state have been investigated at 10 K.

## II. Experimental Section

$PbWO_4:Pr^{3+}$ single crystal has been grown from the melt by the Czochralski method. The doping concentration was 2.0 at. %. The raw materials were 5N PbO and $WO_3$ powders prepared in the precise stoichiometric ratio. The impurities were analyzed by glow discharge mass spectroscopy (GDMS) method, indicating that the concentrations of impurity ions such as $Mo^{6+}$, $Ca^{2+}$, $Fe^{2+}$, $Na^+$, $K^+$, etc. were below 0.5 ppm. The crystal plate of $10 \times 10 \times 5$ mm$^3$ was in dimensions, with its large faces normal to the crystal *c*-axis. Optical absorption spectra were measured with a Shimazu-2501.

The excitation source is a Dye laser (Spectron Laser Sys. SL4000) pumped by the second harmonic (532 nm) of a pulsed Nd:YAG (yttrium aluminum garnet) laser (Spectron Laser Sys. SL802G). The laser beam was focused inside the sample with a cross-sectional area of about 3 mm$^2$. The pulse energy was about 5 mJ with 10 Hz repetition rate and 5 ns duration. The samples were placed in a liquid helium flow cryostat for measurements in the variable-temperature region (10−300 K). The luminescence was dispersed by a 75 cm monochromator (Acton Research Corp. Pro-750) and observed with a photomultiplier tube (PMT) (Hamamatsu R928) with which the signal is detectable up to about 850 nm. Suitable filters were used to eliminate the intense scattering peaks in the spectrum due to the scattered laser irradiation. Photoluminescence spectra were also measured at various temperatures between 10 K and 300 K with a Spex Fluorolog-3 fluorophotometer. The excitation source was a 450 W Xe lamp.

## III. Results and Discussion

**Emission from $^3P_J$ ($J = 0, 1, 2$) Levels.** Figure 1a−c is the emission spectra of $Pr^{3+}$ ions in $PbWO_4$ crystal under excitation of 447 nm ($^3P_2$), 473 nm ($^3P_1$) and 488 nm ($^3P_0$), respectively. It can be seen that, the $^3P_0$ level shows its predominantly radiative character with the typical greenish-blue luminescence in $PbWO_4$ crystal. Under excitation at $^3P_2$, $^3P_1$ and $^3P_0$ levels, $Pr^{3+}$ ions doped in $PbWO_4$ exhibit the emission mainly from the $^3P_0$ manifold, such as the intensive emissions from the $^3P_0 \rightarrow {}^3H_6$ and $^3P_0 \rightarrow {}^3F_2$ transitions around 619 and 648 nm, respectively, and some weak emissions related to other transitions from $^3P_J$ ($J = 0, 1, 2$) manifolds.

The emission spectra, which were obtained by the excitation into the $^3P_2$ level, consist of several lines corresponding to the transitions $^3P_0 \rightarrow {}^3H_{4,5,6}$, $^3P_0 \rightarrow {}^3F_{2,3,4}$ (Figure 1a). The most intense emission is due to the $^3P_0 \rightarrow {}^3F_2$ transition, and the $^3P_1$ emission (marked with asterisk in Figure 1a) was not observed at low temperature (10 K) but could be detected only at room temperature. Under the excitation into the $^3P_1$ levels (Figure 1b), the $^3P_1$ levels show intensive emission, especially at room temperature, together with the $^3P_0$ emission. Similarly, emissions from $^3P_1$ could be also observed under excitation into $^3P_0$ at 300 K (Figure 1c) due to the thermal population of $^3P_1$ through $^3P_0$. For example, although the gap between $^3P_0$ and $^3P_1$ is 635 cm$^{-1}$, the emission from $^3P_1$ could be still observed at 300 K. Moreover, the emission lines from $^3P_1$ have the similar lifetime as $^3P_0$ at a temperature from the room temperature to 150 K, which means that these levels are in thermal equilibrium. However, at low temperatures (10−100 K), the fluorescence from $^3P_1$ level only could be observed under excitation in $^3P_1$ states but not in the $^3P_0$ and $^3P_2$ level.

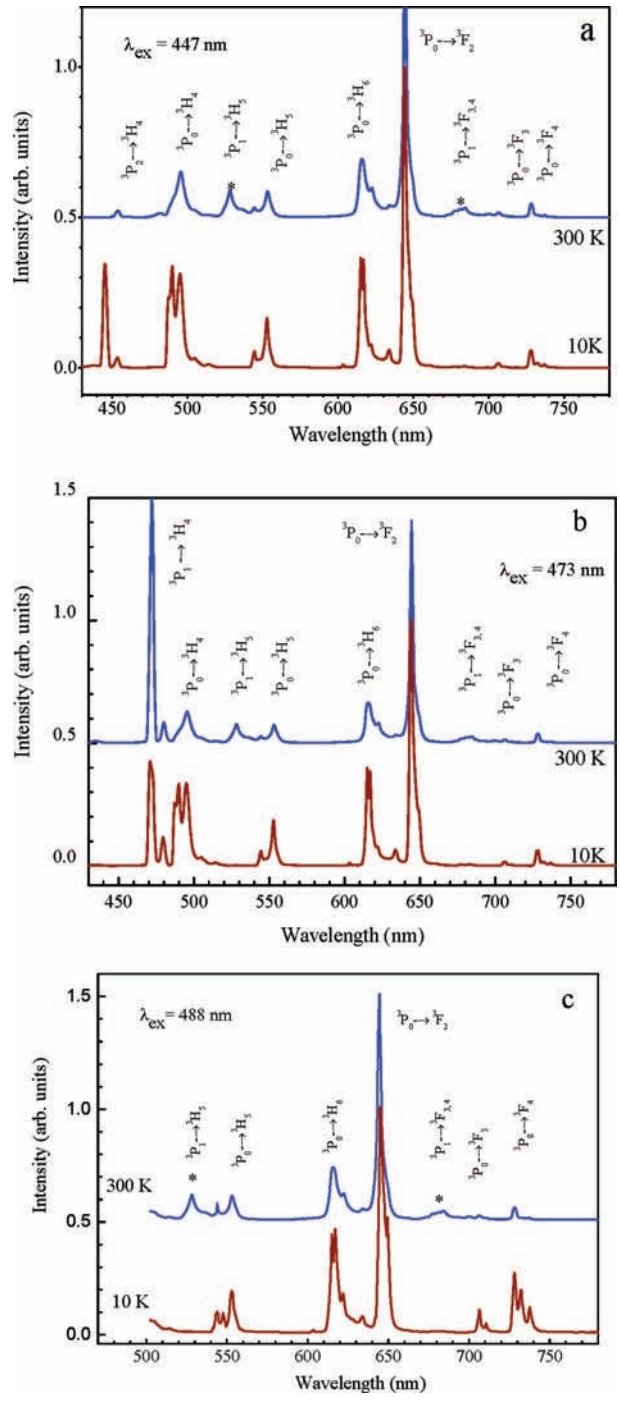


**Figure 1.** Emission spectra of $Pr^{3+}$ ions in $PbWO_4$ crystal under excitation, (a) 447 nm, (b) 473 nm, and (c) 488 nm, at 10 and 300 K.

The fluorescence decay was obtained under excitation at 473 nm ($^3P_1$, decided from absorption spectrum), 488 nm ($^3P_0$), and 592 nm ($^1D_2$) by collecting at emission from ($^3P_1 \rightarrow {}^3H_4$), ($^3P_0 \rightarrow {}^3F_2$), and ($^1D_2 \rightarrow {}^3H_4$) at different temperatures. Table 1 lists the lifetimes of $^3P_1$, $^3P_0$ and $^1D_2$. Figure 2 shows, as an example, the experimental decay curves for $^3P_1$ and $^3P_0$ states at lower temperature together with the fit to the exponential function.

At all temperatures measured, the decay profiles of the $^3P_1$ and $^3P_0$ levels remain single exponential, which has a similar lifetime with values of 2.45 $\mu$s ($^3P_1$) and 2.53 $\mu$s ($^3P_0$) at room temperature. At a lower temperature, they show a difference. The $^3P_1$ and $^3P_0$ states fluoresce and have a lifetime value of 2.03 $\mu$s ($^3P_1$) and 3.34 $\mu$s ($^3P_0$), respectively (Figure 2). The

**TABLE 1: Lifetimes ($\mu$s) of the $^3P_1$, $^3P_0$, and $^1D_2$ Levels Obtained under Different Excitation and at Different Temperatures**

| | | | $\lambda_{ex}$ = 590.27 nm | | |
|---|---|---|---|---|---|
| temp, K | $\lambda_{ex}$ = 470 nm $^3P_1$ | $\lambda_{ex}$ = 488 nm $^3P_0$ | $^3P_1$ | $^3P_0$ | $^1D_2$[a] |
| 10 | 2.03 | 3.30 | $\tau_r = 0.24$<br>$\tau_d = 3.99$ | $\tau_r = 0.85$<br>$\tau_d = 5.71$ | 36.36 |
| 100 | 2.15 | 2.87 | | $\tau_r = 0.75$<br>$\tau_d = 5.12$ | 30.15 |
| 300 | 2.45 | 2.53 | | $\tau_r = 0.69$<br>$\tau_d = 3.58$ | 12.22 |

[a] The lifetime value correspond to the average lifetime.

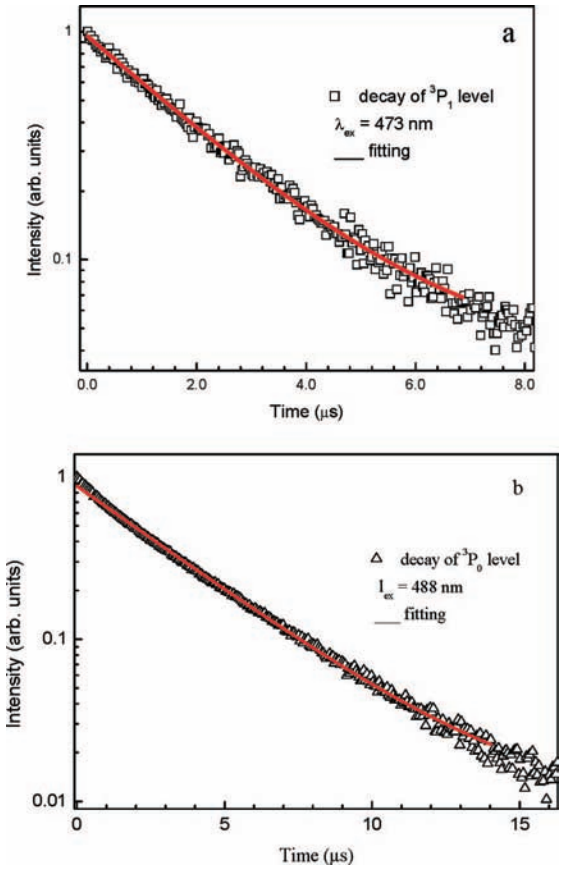


**Figure 2.** Fluorescence decay curves of (a) $^3P_1$ levels under excitation at 473 nm and (b) $^3P_0$ levels under excitation at 488 nm. Symbols correspond to experimental data and the solid line is the fit to a single exponential. All were measured at 10 K.

decay curve of $^3P_0$ is exponential and does not have great differences at 10 and 300 K. According to the Judd−Ofelt (J−O) calculation in the $PbWO_4$:$Pr^{3+}$ crystal,[18] the fluorescence quantum efficiency of $^3P_0$ states is higher than 74 % at room temperature, which was explained to be the reason for the smaller phonon energy of the $(WO_4)^{2-}$ group (about 900 $cm^{-1}$) and the relatively weak the multiphonon relaxation.[7]

**Emission from the $^1D_2$ Level.** As mentioned above, the fluorescence of $^1D_2$ states have not been detected at any temperature by exciting into $^3P_J$ ($J$ = 0, 1, 2) levels. The experiments show that the emission from the $^1D_2$ was only observed under resonant pumping this level itself. According to the model developed by Riseberg and Moos,[20] the rate of energy transfer due to a multiphonon process in an idealized single phonon model is given by

$$W = W_0(1 - e^{-E/kT})^{-p} \quad (1)$$

where $p$ is the number of phonons with energy $E$. The energy separation between the $^3P_0$ and $^1D_2$ manifolds is about 3700 $cm^{-1}$. Therefore it is suggested that the multiphonon relaxation from the $^3P_0$ manifold to the next-lower $^1D_2$ manifold is weak. According to the J−O calculation results, the fluorescence branching ratios for the $^3P_0 \rightarrow {}^1D_2$ and $^3P_0 \rightarrow {}^1G_4$ transitions are very small (about 0.03% and 0.7%, respectively). So, the fluorescence emissions from the $^1D_2$ and $^1G_4$ manifolds can hardly be observed in Figure 1. And the $^3P_0$ lifetime has a smaller changing by a multi-phonon process at temperature between 10 and 300 K.

The photoluminescence properties of infrared emission from $^1D_2$ manifolds are also checked. As shown in Figure 3, under excitation of a 592 nm Xe lamp at 10 K, stronger infrared emission from $^1D_2$ manifolds to $^3F_J$ and $^1G_4$ could be observed. Each of the infrared emission bands increases with decreasing temperature as shown in Figure 4. Figure 5 shows the excitation spectra for 1038 nm $^1D_2 \rightarrow {}^3F_4$ emission at 10 and 296 K. At 296 K, the$^1D_2$ state shows a broad absorption band. At 10 K, it presents two separated absorption peaks with energy levels of 590.3 nm and 599.5 nm. The excitation spectrum for $^1D_2 \rightarrow {}^3F_4$ transition (1038 nm) also shows that the infrared emission is generated from the excitation of not only the $Pr^{3+}$ ions but also the host $PbWO_4$ as seen from the band at 350 and 280 nm. This confirms the excitation energy transfer from PWO host to the 4f shell of $Pr^{3+}$ ions. Similar conclusion has been reported in detail in $Er^{3+}$ doped PWO single crystals.[6]

**Quenching of the $^1D_2$ Level.** The fluorescence emission from the $^1D_2$ level was only observed by resonant pumping of this level. Figure 6 shows the fluorescence spectrum in the region 590−650 nm under $^1D_2$ direct excitation at 590.27 nm at 10 K. Checking the decay profile and lifetime of each fluorescence lines in this spectra region under direct pumping into $^1D_2$ levels reveals two components, which contribute to these red emission bands. The emission from 590 to 615.50 nm corresponds to the $^1D_2 \rightarrow {}^3H_4$ transitions (with a longer decay) with an intensive emission at 603.86 nm and the other weak emission lines from the $^1D_2 \rightarrow {}^3H_4$ transitions. On the other hand, the experimental results indicate that the emission from 616.84 to 650 nm arises from the $^3P_0$ states populated via an up-conversion process in short decay and rise times, as shown later.

Unlike the emission due to the $^3P_0 \rightarrow {}^3H_4$ transition, the decay curves of the emissions due to the $^1D_2 \rightarrow {}^3H_4$ transitions do not give a single exponential at any temperature, as seen in Figure 7. This figure shows the fluorescence decay curves of $^1D_2$ levels

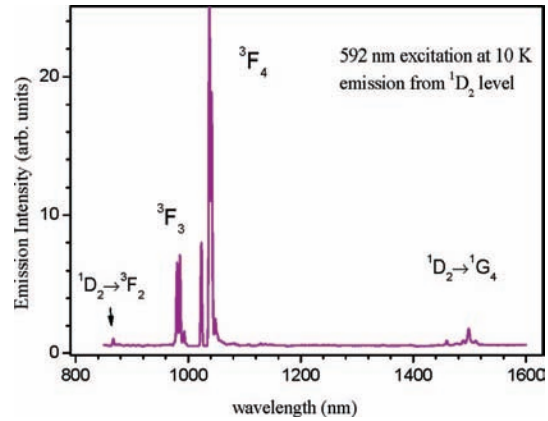


**Figure 3.** Infrared emission spectrum of $Pr^{3+}$ doped in $PbWO_4$ under excitation of a 592 nm Xe lamp at 10 K.

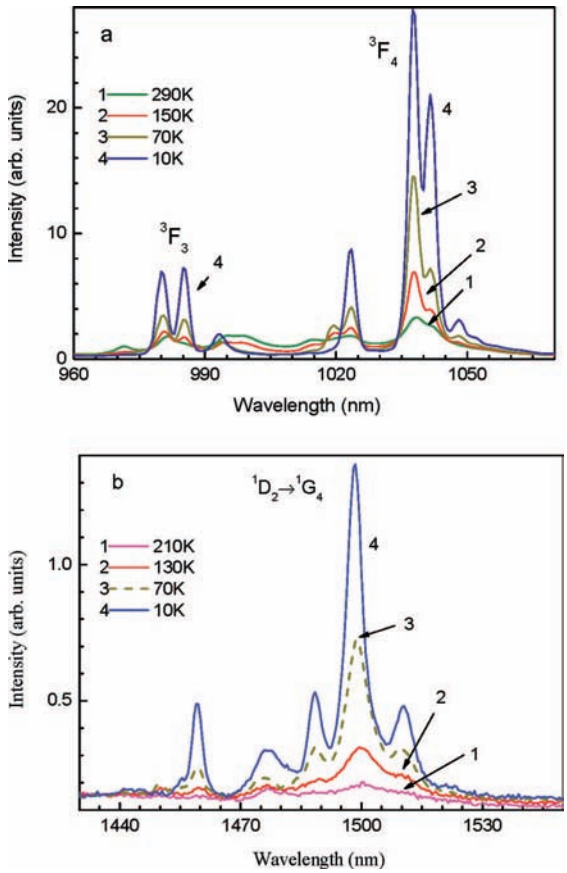


**Figure 4.** Temperature dependence of infrared emission spectra of $PbWO_4:Pr^{3+}$ excited with a 592 nm Xe lamp at different temperature.

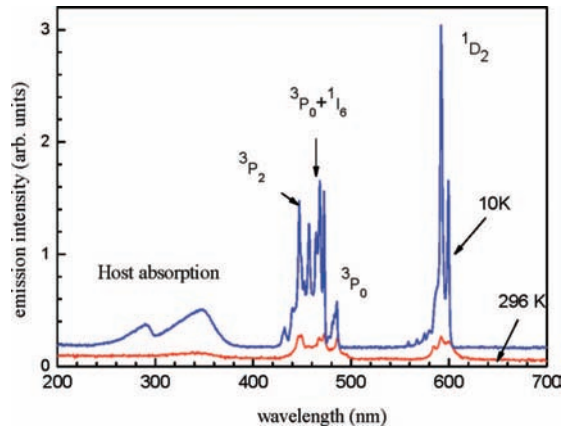


**Figure 5.** Excitation spectra for 1038 nm $^1D_2 \rightarrow {}^3F_4$ emission at 10 and 296 K.

obtained under direct pumping into $^1D_2$ levels at 590.27 nm at 300 K (a) and 10 K (b). The lifetimes are calculated as an average value and listed in Table 1.

The characteristic decay process of the $^1D_2$ state of $Pr^{3+}$ ions is governed by a sum of probabilities for several competing processes: radiative decay, nonradiative decay by multiphonon emission, and nonradiative decay by energy transfer to other $Pr^{3+}$ ions.[21] The nonradiative decay by multiphonon emission from the $^1D_2$ level is expected to be small because of the large energy gap to the next $^1G_4$ lower level (7297 $cm^{-1}$) as compared with the highest energies of the phonons involved (about 900 $cm^{-1}$).

In this highly-doped crystal, inter-ion $Pr^{3+}-Pr^{3+}$ relaxation process plays an important role, leading to (1) cross-relaxation

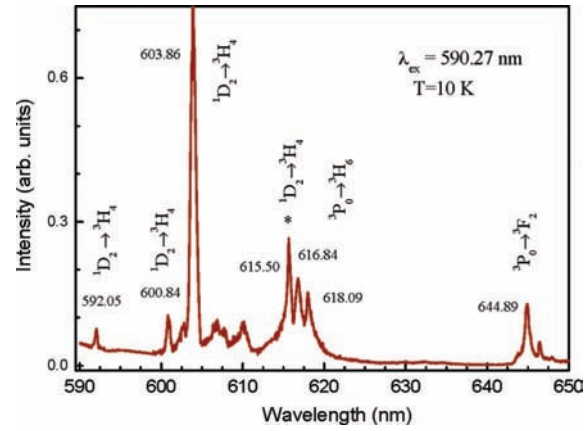


**Figure 6.** Fluorescence spectra of $Pr^{3+}$ in $PbWO_4$ in the region 590−650 nm under direct pumping into $^1D_2$ levels at 590.27 nm at 10 K.

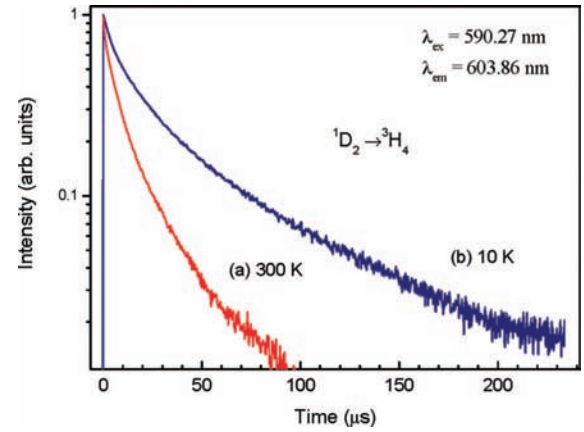


**Figure 7.** Fluorescence decay curves of $^1D_2$ levels under direct pumping into $^1D_2$ levels at 590.27 nm at 300 K (a) and 10 K (b).

between pairs of $Pr^{3+}$ ions and (2) migration of the excitation energy due to resonant energy transfer among $Pr^{3+}$ ions until reaching a quenching centre. Usually, in a highly-doped sample (increases up to 1.0 mol %), the change from exponential to nonexponential decays of $^1D_2$ levels could be mainly due to energy diffusion and cross-relaxation processes.[21] To identify the energy transfer between $Pr^{3+}$ ions, the experimental decays of the $^1D_2$ level have been analyzed by the continuum model proposed by Inokuti and Hirayama[22] as the expression

$$I(t) = I(0)\exp\left[-\frac{t}{\tau_0} - \Gamma\left(1-\frac{3}{s}\right)\frac{4}{3}\pi R_0{}^3 N\left(\frac{t}{\tau_0}\right)^{s/3}\right] \quad (2)$$

$N$ is the acceptor concentration, $R_0$ is the critical transfer distance for which the probability for energy transfers between a donor and acceptor is equal to the intrinsic decay probability $1/\tau_0$. $\Gamma(t)$ is the gamma function of $t$, and $s = 6$, 8, and 10 correspond to electric dipole−dipole, dipole−quadrupole, and quadrupole−quadrupole energy-transfer mechanisms, respectively. The intrinsic decay time is adopted from the J−O calculation as 38.50 $\mu$s.[18] The fluorescence decay curve of the $^1D_2 \rightarrow {}^3H_4$ transition is analyzed as $[I(t)/I(0)] + t/\tau_0$ against $(t_0)^{3/s}$ and linear fitting for $s = 6$, 8, and 10 based on the Inokuti−Hirayama model. In all cases the best fit was for $s = 6$ for all temperatures (Figure 8). The critical transfer radius is obtained to about 1.05 nm. This value is close to the value of 1.07 nm obtained in $PbWO_4$ doped with 1.50 at % $Pr^{3+}$ ions.[18] This indicates that the cross-relaxation energy transfer is caused by the electric dipole−dipole transfer mechanism and is responsible for the

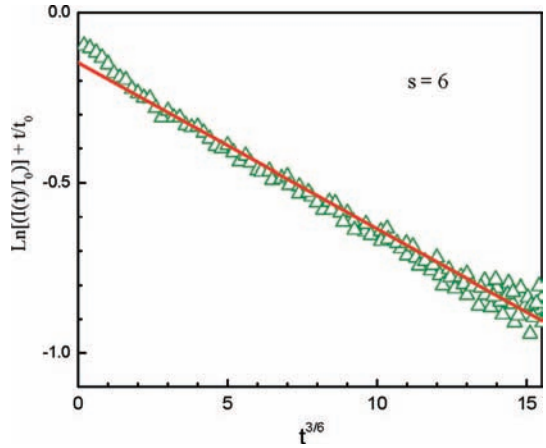


**Figure 8.** Logarithmic plot of the experimental emission decay curves of the level $^1D_2$ at 10 K, and the fit for dipole−dipole interaction ($s = 6$).

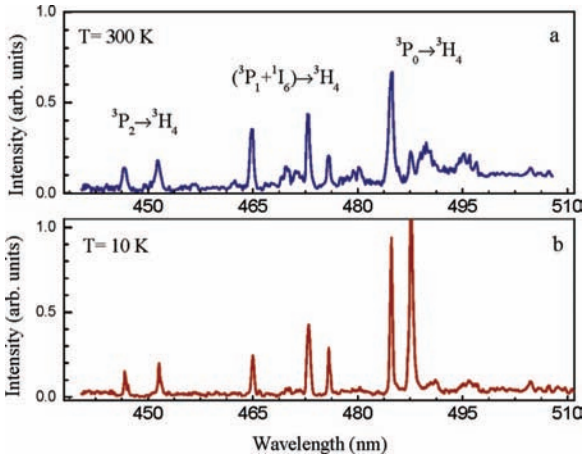


**Figure 9.** Up-conversion fluorescence spectra corresponding to the $^3P_1$, $^3P_0 \rightarrow {}^3H_4$ transition at (a) 300 K and (b) 10 K. The excitation wavelength (590.27 nm) was in resonance with the transition $^3H_4 \rightarrow {}^1D_2$.

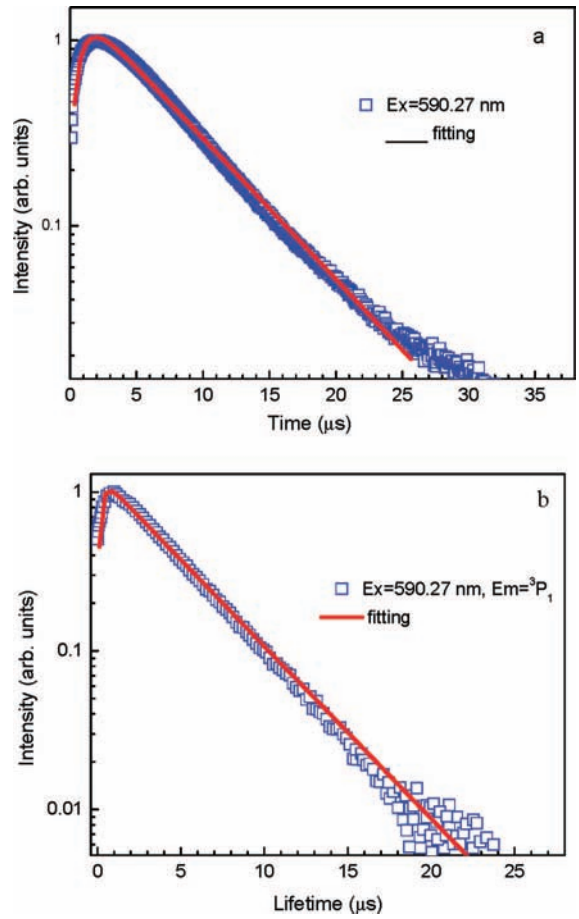


**Figure 10.** Experimental emission decay curves in a semilogarithmic representation of level $^3P_0$ (a) and level $^3P_1$ (b), obtained under excitation in resonance with the transition $^3H_4 \rightarrow {}^1D_2$ (590.27 nm) at 10 K. Symbols correspond to experimental data and the solid line is the fit to eq 3.

nonexponential character of the fluorescence decay from the $^1D_2$ manifold of $Pr^{3+}$ ions in $PbWO_4$. Therefore it is suggested that the fluorescence emission from the $^1D_2$ manifold of $Pr^{3+}$ in $PbWO_4$ crystal is strongly influenced by a nearly resonant cross-relaxation process. The process has also been observed for transitions $^1D_2 \rightarrow ({}^1G_4, {}^3F_4)$ and $^3H_4 \rightarrow ({}^1G_4, {}^3F_4)$ in the other $Pr^{3+}$-doped crystals.[23]

**Orange-to-Blue Frequency Up-Conversion and Assignments.** The existence of orange-to-blue up-converted fluorescence in this $Pr^{3+}$-doped $PbWO_4$ crystal has been investigated by directly exciting the $^1D_2$ level. The anti-Stokes fluorescence from the $^3P_1$ and $^3P_0$ levels has been observed at 10−300 K by exciting in resonance with the $^3H_4 \rightarrow {}^1D_2$ transition at 590.27 nm (Figure 9). The up-conversion emission due to $^3P_0 \rightarrow {}^3H_4$ consists of two clear peaks at low temperature as seen in Figure 9. Of the two emission lines, one emission line at about 488 nm is greatly quenched at 300 K. This might be caused by the complex structure defects in this Scheelite crystal.[4]

In general, the up-conversion process can occur via three possible processes: namely, excited state absorption (ESA), energy-transfer up-conversion (ETU), and photo avalanche up-conversion processes.[24] Here the photo avalanche up-conversion could be excluded because no pump power threshold for up-conversion luminescence was observed at any temperature. As for the $Pr^{3+}$-doped materials, both the ESA and ETU processes have been observed for the up converted blue emission from the $^3P_0$ level after orange excitation at level $^1D_2$.[25,26] In the first processes a single ion is involved, whereas two ions are involved in the second one.

For all up-conversion in this experiment, the intensity of the anti-Stokes emission shows a quadratic dependence on the excitation laser energy, indicating that two photons participate in this process. Lifetime measurements provide a useful tool to determine which process is really working. The radiative ESA process occurs within the excitation pulse width, leading to an immediate decay of the up-conversion luminescence after excitation. Up-conversion by energy transfer leads to a decay curve for the anti-Stokes emission which shows a rise time after the laser pulse, followed by decay and a longer lifetime than that of level $^3P_0$ under direct excitation.

An example is shown in Figure 10 which presents the experimental decay curves of level $^3P_0$ and $^3P_1$ obtained at 10 K. All the decay curves obtained by exciting at 590.27 nm and have a rise time and a decay lifetime which is much longer than that of the level $^3P_0$ (5.72 $\mu$s) and $^3P_1$ (3.99 $\mu$s) under direct excitation. At the other temperature, the decay curve has the same profile. The observed rise time of the $^3P_0$ and $^3P_1$ decays obtained under pulsed excitation in the $^1D_2$ state indicates that the energy-transfer process seems to be mainly responsible for the anti-Stokes fluorescence of $Pr^{3+}$ in this crystal. The similar behavior has been found in the other crystals, e.g., $LaF_3$:$Pr^{3+}$ and $KPb_2Cl_5$:$Pr^{3+}$, and $Pr^{3+}$-doped glass, which was attributed

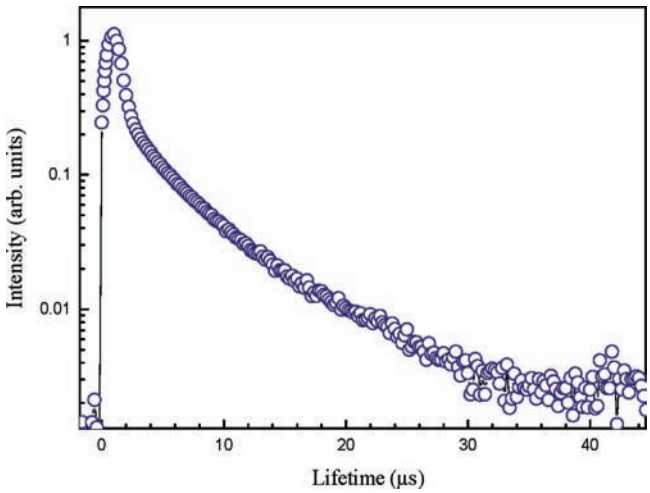


**Figure 11.** Experimental emission decay curve in a semilogarithmic representation of emission lines of 616.84, 618.09 and 644.89 nm in Figure 6 from the $^3P_0$ level, obtained under excitation in resonance with the transition $^3H_4 \rightarrow {}^1D_2$ (590.27 nm) at 10 K.

to a redistribution of energy between two ions according to $^1D_2 + {}^1D_2 = {}^1G_4 + {}^3P_2$ phonons.[27–29] According to Buisson and Vial,[30] energy transfer occurs when two $Pr^{3+}$ ions are excited to the $^1D_2$ state: one ion is excited to the lower excited level $^1G_4$, and the other ion is excited to the $^3P_2$ level by nonradiative decay. As a result the $^3P_0$ and $^3P_1$ level are populated. The rise and decay time were obtained by fitting the curve to the following equation:

$$I(t) = k(e^{-t/\tau_d} - e^{-t/\tau_r}) \quad (3)$$

where $k$ is a constant, $\tau_d$ is the decay time, and $\tau_r$ is the rise time. In this model, $\tau_r$ is decided by the decay time of the $^3P_J$ ($J = 0, 1, 2$) state, whereas $\tau_d$ should be determined by the decay time of the $^1D_2$ level and the energy-transfer rate.

Figure 10a,b shows the fitting of the experimental decay to eq 3. Good fit of the experimental decay to eq 3 is obtained. All the decay curves of the $^3P_1$ and $^3P_0$ emissions, which were obtained by excitation into the $^1D_2$ state at 590.27 nm, show a rise time and a decay lifetime. These times are much longer than those of the $^3P_1$ and $^3P_0$ level obtained under direct excitation. The values of $\tau_d$ and $\tau_r$ are listed in the Table 1.

On the basis of the lifetime measurements, a direct two-photon absorption process is unlikely, because this processes would require that the upconverted fluorescence decay of the $^3P_0 \rightarrow {}^3H_4$ transition be identical to the lifetime of the directly excited $^3P_0$ and $^3P_1$ levels. As shown in Table 1, the observed lifetime of the induced upconversion fluorescence (at 10 K, 5.71 $\mu$s for $^3P_0$ and 3.99 $\mu$s for $^3P_1$ levels) is about twice as large as the lifetime observed for the directly exciting (3.30 $\mu$s for $^3P_0$, and 2.03 $\mu$s for $^3P_1$ levels). The existence of rise times in the red emission decays confirms that this emission is produced through some energy-transfer process.

From the decay profile and lifetime, the observed fluorescence emission lines of 616.84, 618.09 and 644.89 nm (Figure 6) are suggested to arise from the $^3P_0$ states populated via an up-conversion process, because these emissions show a rise time. Figure 11 shows the decay profiles at 10 K. This emission shows an obvious rise time (0.69 ms); however, the following decay is not an exact exponential decay curve with an average lifetime of 3.58 ms. This indicates that the emission originates from up-conversion and has a complex radiative transition after different relaxation processes where the $^3P_J$ ($J = 0, 1, 2$) levels are

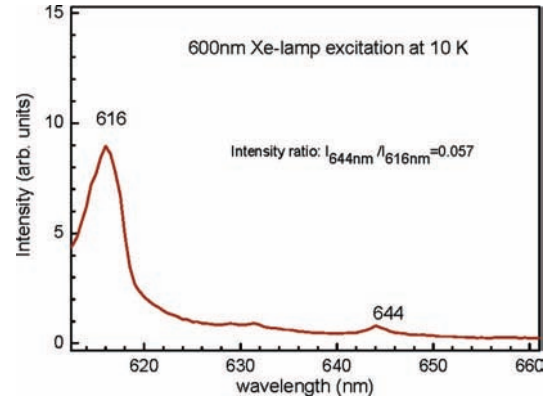


**Figure 12.** Emission spectrum by a 600 nm Xe-lamp excitation.

involved. And moreover, from Figure 6, which was obtained by laser excitation, it is estimated that the 644.89 nm peak height is about 0.5 of the 615.50 nm peak height (intensity ratio: $I_{644nm}/I_{616nm} = 0.5$), whereas from Figure 12, which was obtained by 600 nm Xe-lamp excitation, it is estimated that the 644 nm peak height is about 0.057 of the 616 nm peak height (intensity ratio: $I_{644nm}/I_{616nm} = 0.057$). This confirms that the assignment of the 644 nm emission to the up-conversion from the $^3P_0$ level is reasonable because a high-power light source such as a laser is necessary to obtain the up-conversion efficiently.

As mentioned above, the energy-transfer up-conversion proceeds according to a scheme in which two ions excited in an intermediate state in close proximity are coupled by a nonradiative process in which an ion returns to the ground state and the other ion is to the upper level. In most cases, these cross relaxation processes are based on electric dipole−dipole interaction,[31] which has been confirmed in the $Pr^{3+}$-doped crystal (Figure 8). Similar energy-transfer up-conversion processing has been confirmed in $Er^{3+}$-doped $PbWO_4$ crystal.[32]

The energy-transfer process is confirmed by the charge compensation in $RE^{3+}$ highly doped $PbWO_4$. $PbWO_4$ crystal with Scheelite structure can accommodate large concentration trivalent rare earth ($RE^{3+}$) ions to ameliorate its scintillation.[4] $La^{3+}$ highly doped $PbWO_4$, e.g., $Pb_{0.7}La_{0.3}WO_{4.15}$, can still keep Sheelite structure well.[33] It has been demonstrated that $RE^{3+}$ doped in an appropriate level would occupy the $Pb^{2+}$ site and induce excess positive charge, which is compensated by $V_{Pb}$ (Pb vacancy) through the formation of defect complexes $[2(RE^{3+}{}_{Pb})^{\bullet}-V_{Pb}'']$.[34,35] $RE^{3+}$ heavily doped PWO have also been extensively investigated. For example, on La heavy doping, $La^{3+}$ might also substitute the W sites besides the $Pb^{2+}$ sites for self-compensation by the formation of La dimers $[(La_W)'''-(La_{Pb})^{\bullet}]-(Vo)^{\bullet\bullet}$ or $La^{3+}$ small aggregates $[3(La_{Pb})^{\bullet}-(La_W)''']$.[36,37] Another charge compensator, the interstitial oxygen ions, might also be involved $[2(RE^{3+}{}_{Pb})^{\bullet}-O_i'']$.[36] This doping mechanism also can be applied for Pr doped $PbWO_4$. For example, the charge compensation and doping mechanism can yield a small $Pr^{3+}-Pr^{3+}$ distance in $PbWO_4$ lattice, leading to quenching of emission by cross relaxation and ET up-conversion processes.

## IV. Conclusion

Optical absorption, the visible luminescence emission spectra of $Pr^{3+}$ ions at temperatures between 10 and 300 K has been analyzed. Strong visible luminescence is observed either from levels $^3P_1$, $^3P_0$ under excitation in $^3P_2$ state or from excitation under level $^1D_2$ at 590.27 nm. The $^3P_0$ level of $Pr^{3+}$ ions shows its predominantly radiative character with the typical greenish-blue luminescence. Emission from level $^1D_2$ is only observed

when this level is directly excited. Under site-selective excitation into $^1D_2$ states by pulsed dye laser, the presence of the complex structures of the emission spectra and different decay profiles indicate the processes that contribute to the quenching of the $^1D_2$ fluorescence of $Pr^{3+}$ ions, i.e., the cross-relaxation and energy-transfer up-conversion luminescence processes from the $^1D_2$ states. The time evolution of the decays from the $^1D_2$ state is consistent with a dipole−dipole energy-transfer mechanism. The nonexponential character of the fluorescence decay curve of the $^1D_2$ manifold can be attributed to a nearly resonant cross-relaxation energy transfer. Under the site-selective excitation in $^1D_2$ states, the anti-Stokes fluorescence from the green ($^3P_0$, $^3P_1$) → $^3H_4$ transition populated via an up-conversion process is first reported. The up-conversion fluorescence intensity has a quadratic dependence on the laser input power. The analyses of temporal evolution indicate that an ETU process is responsible for the up-converted luminescence.

**Acknowledgment.** This work was financially supported by Jiangsu Provincial Natural Science Foundation of China (BK-2007053) and the Korea Research Foundation Grant funded by the Korean Government (MOEHRD, Basic Research Promotion Fund) (KRF-2007-313-C00312). T.T. is thankful for support by a Grant-in-Aid for Joint Research Project under the Japan/Korea Joint Committee for Basic Science Research, which is established by Korea Science and Engineering Foundation (KOSEF) and the Japan Society for the Promotion of Science (JSPS).

## References and Notes

(1) CMS Collaboration. The Electromagnetic Calorimeter Technical Design Report CERN/LHCC. **1977**, *97−33*, 43.
(2) Lecoq, P. *Nucl. Instrum. Methods Phys. Res. A* **2005**, *537*, 15.
(3) Kobayashi, M.; Usuki, Y.; Ishii, M.; Yazawa, T.; Hara, K. *Nucl. Instrum. Methods Phys. Res. A* **1997**, *399*, 261.
(4) Nikl, M. *Phys. Status Solidi A* **2000**, *178*, 595.
(5) Geng, J.; Lu, D.; Zhu, J.; Chen, H. *J. Phys. Chem. B* **2006**, *110*, 13777.
(6) Huang, Y.; Feng, X. *J. Phys. D: Appl. Phys.* **2003**, *36*, 1783.
(7) Kaminskii, A.; Eichler, H.; Ueda, K.; Klassen, N.; Redkin, B.; Li, L.; Findeisen, J.; Jaque, D.; Garca-Sole, J.; Fernandez, J.; Balda, R. *Appl. Opt.* **1999**, *38*, 4538.
(8) Kaminskii, A.; McCray, C.; Lee, H.; Lee, S.; Temple, D.; Chyba, T.; Marsh, W.; Barnes, J.; Annanenkov, A.; Legun, V.; Eichler, H.; Gad, G.; Ueda, K. *Opt. Commun.* **2000**, *183*, 277.
(9) Chen, W.; Inagawa, Y.; Omatsu, T.; Tateda, M.; Takeuchi, N.; Usuki, Y. *Opt. Commun.* **2001**, *194*, 401.
(10) Kaminskii, Alexander A. *Laser Photon. Rev.* **2007**, *1*, 93–177.
(11) Funk, D. S.; Eden, J. G.; IEEE, J. *Sel. Top. Quantum Electron.* **1995**, *1*, 784.
(12) Petreski, B. L.; Farrell. P.M.; Collins, S.F. *Fiber and Integrated Optics*; Taylor and Francis: Melbourne, 1999.
(13) Shi., Y.; Poulsen, C.V.; Sejka, M.; Ibsen, M.; Poulsen, O. *Electron. Lett.* **1993**, *29*, 1426.
(14) Kaminskii, A. A.; Kurbanov, K.; Ovanesyan, K. L.; Petrosyan, A. G. *Phys. Stat. Sol. (a)* **1988**, *105*, K155.
(15) Kaminskii, A. A.; Kurbanov, K.; Uvarova, T.V. *Inorg. Mater.* **1987**, *23*, 940.
(16) Kaminskii, A. A.; Li, L.; Butashin, A.V.; Mironov, V. S.; Pavlyuk, A. A.; Bagayev, S. N.; Ueda, K. *Opt. Rev.* **1997**, *4*, 309.
(17) Antonenko, O.; Chukova, O.; Hizhnyi, Yu.; Nedilko, S.; Scherbaskyi, V. *Opt. Mater.* **2006**, *28*, 643.
(18) Xiong, F.; Luo, Z. Huang, Y. *Appl. Phys. B: Laser Opt.* **2005**, *80*, 321.
(19) Xiong, F.; Lin, Y.; Chen, Y.; Luo, Z.; Ma, E.; Huang, Y. *Chem. Phys. Lett.* **2006**, *429*, 410.
(20) Riseberg, L.; Moos, H. *Phys. Rev.* **1968**, *174*, 429.
(21) Balda, R.; Sáez, de.; Fernández, J.; Fdez-Navarro, J.; Arriandiaga, M. *J. Phys.: Condens. Matter* **2000**, *12*, 10623.
(22) Inokuti, M.; Hirayama, F. *J. Chem. Phys.* **1965**, *43*, 1978.
(23) Savoini, B.; Santiuste, J.; Gonzalez, R. *Phys. Rev. B* **1997**, *56*, 5856.
(24) Auzel, F. *Proc. IEEE* **1973**, *61*, 758.
(25) Malta, O.; Antic-Fidancev, E.; Lemaitre-Blaise, M.; Dexpert-Ghys, J.; Piriou, B. *Chem. Phys. Lett.* **1986**, *129*, 557.
(26) Balda, R.; Fernandez, J.; Saez de Ocariz, I.; Voda, M.; Garca, A.; Khaidukov, N. *Phys. Rev. B* **1999**, *59*, 9972.
(27) Vial, J.; Buisson, R.; Madeore, F.; Poirier, M. *J. Phys.* **1979**, *40*, 913.
(28) Balda, R.; Voda, M.; Al-Saleh, M.; Fernandez, J. *J. Luminescence* **2002**, *97*, 190.
(29) Fernández, J.; Balda, R.; Mendioroz, A.; Garcí-Adeva, A. J. *Phys.: Condens. Matter* **2001**, *13*, 10347.
(30) Buisson, R.; Vial, J. *J. Phys. Lett.* **1981**, *42*, L115.
(31) Capobianco, J.; Raspa, N.; Monteil, A.; Malinowski, M. *J. Phys.: Condens. Matter* **1993**, *5*, 6083.
(32) Huang, Y.; Seo, H.; Yang, Y.; Zhang, J. *Mater. Chem. Phys.* **2005**, *91*, 424.
(33) Esaks, T.; Mina-ai, T.; Iwahara, H. *Solid State Ionics* **1992**, *57*, 319.
(34) Li, W.; Tang, T.; Huang, H.; Feng, X. *Jpn. J. Appl. Phys.* **2001**, *40*, 6893.
(35) Han, B.; Feng, X.; Hu, G.; Wang, P.; Yin, Z. *J. Appl. Phys.* **1998**, *84*, 2831.
(36) Zhu, W.; Feng, X.; Huang, Y.; Lin, Q. *Phys. Stat. Sol. (a)* **2002**, *193*, 211.
(37) Huang, Y.; Zhu, W.; Feng, X. *J. Solid State Chem.* **2003**, *172*, 188.

JP712030Q